https://doi.org/10.1016/j.ijhydene.2020.12.115

Unveiling the role of hydrogen on the creep behaviors of nanograined α-Fe via molecular dynamics simulations

Xiao-Ye Zhou[a], Ji-Hua Zhu[a*], Hong-Hui Wu[b*], Xu-Sheng Yang[c, d], Shuize Wang[b], Xinping Mao[b*]

[a] Guangdong Province Key Laboratory of Durability for Marine Civil Engineering, College of Civil and Transportation Engineering, Shenzhen University, Shenzhen, Guangdong 518060, PR China

[b] Beijing Advanced Innovation Center for Materials Genome Engineering, University of Science and Technology Beijing, Beijing 100083, China

[c] Advanced Manufacturing Technology Research Centre, Department of Industrial and Systems Engineering, The Hong Kong Polytechnic University, Hung Hom, Kowloon, Hong Kong

[d] Hong Kong Polytechnic University Shenzhen Research Institute, Shenzhen, China

Corresponding Authors

*Ji-Hua Zhu, E-mail: zhujh@szu.edu.cn

*Hong-Hui Wu, E-mail: wuhonghui@ustb.edu.cn

*Xinping Mao, E-mail: maoxinping@ustb.edu.cn

Abstract

Hydrogen embrittlement (HE) substantially deteriorates the mechanical properties of metals. The HE behavior of nanograined (NG) materials with a high fraction of grain boundaries (GBs) may significantly differ from those of their coarse-grained counterparts. Herein, molecular dynamics (MD) simulations were performed to investigate the HE behavior and mechanism of NG α-Fe under creep loading. The effects of temperature sustained stress, and grain size on the creep mechanism was examined based on the Mukherjee-Bird-Dorn (MBD) equation. The deformation mechanisms were found to be highly dependent on temperature, applied stress, and grain size. Hydrogen charging was found to have an inhibitory effect on the GB-related deformation mechanism. As the grain size increased, the HE mechanism transitioned from H-induced inhibition of GB-related deformation to H-enhanced GB decohesion. The current results might provide theoretical guidance for designing NG structural materials with low HE sensitivity and better mechanical performance.

Keywords: plastic deformation mechanism; molecular dynamics simulations; hydrogen embrittlement; nanograined materials; creep behavior.

1. Introduction

Nanograined (NG) materials, for which the average grain size is less than 100 nm, have attracted great attention due to their unique properties, which are often attributed to their extremely high volume-fraction of grain boundaries (GBs)[1, 2]. For NG materials, GBs can not only impede dislocation motions but can also play a major role in the plastic deformation process. GB-related deformation modes that have been observed in NG metals include grain rotation[3] and GB sliding and migration[3, 4]. Hydrogen embrittlement (HE) is a phenomenon in which the mechanical properties of metals, especially the plasticity and durability, deteriorate substantially due to the hydrogen atoms included in those metals[5-9]. For NG materials, H atoms can interact with GBs in many ways. Studies have shown that hydrogen atoms tend to accumulate at GBs[10] and that GBs—as a strong trap for H atoms—can reduce diffusible H[11, 12]. Moreover, H atoms segregated at GBs can weaken the cohesive energy of GBs, thereby contributing to GB decohesion[13, 14]. Our previous study found that H can greatly influence GB-related deformation by inhibiting GB motions[15]. In addition to the above-mentioned interactions between H atoms and GBs, H atoms can also be trapped at dislocation cores[16], influence dislocation motions[17], or facilitate void formation[18, 19], which consequently influences the deformation of NG materials. Studies have shown that grain refinement can improve HE resistance of metals, owing to the increased amount of GBs[20-27]. The above analysis shows that the HE properties and mechanism of NG materials should largely deviate from those of coarse-grained (CG) materials. As NG materials with different grain sizes have different GB fractions, the HE properties and mechanism of NG materials should be dependent on the grain size. However, current HE mechanisms which focus more on the HE behavior in coarse-grained materials ignore the influences of GBs. Therefore, it is necessary to investigate the HE properties and mechanism of NG materials to understand the GB influence on HE behaviors and assist the design of NG materials

with low HE sensitivity for use in H-containing environments.

The creep behaviors of metals, especially at high temperatures, are essential to their applications. Creep tests performed at different temperatures and sustained stress levels can also help us understand the plastic deformation mechanism[28]. The creep mechanisms within a temperature and stress range can be revealed by determining the corresponding plastic deformation parameters based on the well-known Mukherjee-Bird-Dorn (MBD) equation[29], which is given by

$$\dot{\varepsilon} = A\left(\frac{1}{d}\right)^{p}\left(\frac{\sigma}{\sigma_0}\right)^{n}\exp\left(-\frac{\Delta Q}{k_B T}\right) \quad (1)$$

where $\dot{\varepsilon}$ is the steady-state creep rate, A is a material constant, d is the average grain size, p is the grain size exponent, σ and σ_0 are the sustained and reference stress, n is the stress exponent, ΔQ is the creep activation energy, k_B is the Boltzmann constant, and T is the temperature. The grain size exponent p, stress exponent n, and creep activation energy ΔQ can provide important information to reveal the plastic deformation mechanism[30-32]. By performing a series of creep tests on nanograined and nano twined copper at different temperatures and sustained stress levels, the creep deformation parameters were successfully obtained in previous experiments[28, 30, 31]. It was suggested that as the temperature and sustained stress increased, the creep mechanism transitioned from Coble diffusion[33] to twin boundary migration and finally to dislocation dominated creep mechanism. It also suggests that a particular deformation mechanism can be achieved by controlling the temperature and sustained stress. Therefore, we can perform creep tests at different temperatures and sustained stress levels and observe the influence of H charging on the activities of different deformation mechanisms. By comparing the deformation parameters of H-charged and uncharged NG materials, the influence of H on the deformation mechanisms can be revealed. Besides, by conducting creep tests of nanograined materials of different grain sizes, the grain size exponent, p, and be obtained, and the grain size effect on the H embrittlement behavior of nanograined materials can be evaluated.

Due to the high diffusivity and small radius of H atoms, the observation of H distribution is extremely difficult through experimental methods. Therefore, molecular dynamics (MD) simulations have been widely adopted to study the HE mechanism[34-38]. MD simulation has the advantage of being able to directly observe the interaction of H atoms with crystal defects, including vacancies, dislocations, deformation twins (DTs), and GBs, of NG materials and the evolution of these defects during deformation. MD simulations of tensile tests have been widely used to study the influence of H on plastic deformation modes[15, 39, 40]. However, due to the timescale limitations in MD simulations, the strain rates in the simulated tensile tests are usually higher than 10^7/s, which can result in unreasonably high yield stress and flow stress[41-43] and leaves little time for H atoms to diffuse and interact with the defects. Consequently, it is difficult to determine the influence of H on the nucleation processes of dislocations and DTs or the influence of H segregation at the GBs by performing uniaxial tensile test simulations with high strain rates. MD simulations of creep tests, on the other hand, can potentially overcome the shortcomings of tensile test simulations. As stated above, the deformation mechanism of nanograined materials changes with varying temperature and stress levels. The influence of H charging on the activities of the deformation mechanisms can be revealed by the difference in the corresponding deformation parameters. In addition, the strain rate in the creep tests MD simulation can be reduced to 10^5/s. Although the strain rate is still much higher than that in reality, compared with the strain rate in uniaxial tensile test simulation, this strain rate allows H atoms to segregate at defect sites and renders it possible to observed GB movement, dislocation nucleation, and propagation.

In this study, MD simulations of creep tests were performed to investigate the HE behavior and deformation mechanisms of NG α-Fe with different grain sizes (ranging from 10 nm to 30 nm). The creep test simulations were conducted at temperatures ranging from 300 K to 800 K and stress levels ranging from 3 GPa to 6 GPa. The

wide temperature and stress ranges enable us to observe the transitions among the deformation mechanisms. By fitting the simulation results by the MBD equation, deformation parameters corresponding to different deformation mechanisms were derived successfully. Along with the real-time atomic configurations given by the MD simulation, we clarified the influence of the grain size, temperature, and applied stress on the deformation mechanism of NG α-Fe. Finally, by comparing the deformation parameters and microstructure evolution of the H-charged and uncharged NG α-Fe models, the influence of H on the deformation mechanism has been revealed. Moreover, the influence of H charging on GB-related deformations has also been clarified. The findings of this study will provide a theoretical guideline for the service of NG α-Fe materials in H-containing environments.

2. Methods

NG α-Fe models were built by using 2-D Voronoi tessellation to separate cubic cells into polyhedrons. To simulate NG α-Fe with various grain sizes, we adopted cubic cells with 3 different in-plane (x-y plane) dimensions. The out-of-plane dimension (the z direction) was 10 nm for all models. The 3 NG models had the same grain arrangement and orientations but different average grain sizes. The models with average grain sizes of 10 nm, 20 nm, and 30 nm were denoted as NG-10, NG-20, and NG-30, respectively. The grain orientations were randomly generated, but orientations that created a large degree of lattice mismatch at the periodic boundary along the normal direction were excluded. Periodic boundary conditions were imposed along all directions. The interatomic interaction was described by an embedded-atom method (EAM) potential developed by Ramasubramaniam et al[44]. This EAM potential was developed for H in α-Fe based on density functional theory and can accurately predict H diffusion and trapping at various crystal defects. After building the NG α-Fe models, MD simulations of the annealing processes were performed using LAMMPS software[45] to obtain equilibrium GB structures. To eliminate the point defects

induced by the lattice mismatch along the z direction, the models were first heated to 900 K and held isothermally for 1 ns with a timestep of 0.001 ps. The models were then cooled to 300 K in 0.3 ns. After annealing, the equilibrated structures of the models were obtained, as shown in Fig. 1a-c. Atomic structures were visualized by OVITO software[46] with crystal structures calculated by common neighbor analysis[47]. Because the grain orientations are selected to avoid mismatch along the normal direction, the grains are free of any lattice defects after annealing. The defect mesh and dislocations are calculated by the dislocation extraction algorithm (DXA) in OVITO.

To simulate the H-charged NG models, H atoms were added to the interstitial sites of the annealed NG α-Fe models with the same concentration of 0.7 at. % (denoted as H_1 hereafter). After the insertion of the H atoms, the models were heated to temperatures ranging from 300 K to 800 K to simulate the diffusion of H atoms in the NG α-Fe models. The duration of the diffusion simulations was set to 5 ns to allow the H atoms to fully diffuse to the GBs. The H distributions after the diffusion simulations are displayed in Fig. 1d-f.

Creep test simulations of the H-charged and uncharged NG α-Fe models were then performed at different temperatures and sustained stress levels. For the H-charged samples, the creep simulations were conducted immediately after the diffusion simulation. A group of sustained stresses ranging from 3 GPa to 6 GPa−with a 0.5 GPa interval−were applied to the NG α-Fe models along the x direction. The y and z directions were kept stress free. The duration of each creep simulation was 1 ns. The curves of creep strain versus time were obtained, and the atomic configurations were conserved for further analysis. The creep simulations of the uncharged NG α-Fe models were performed similarly, but the annealed NG α-Fe models were first heated to the corresponding temperature and held isothermally for 0.1 ns. Constant stresses were then applied to the NG models, and the creep simulations were run for 1 ns.

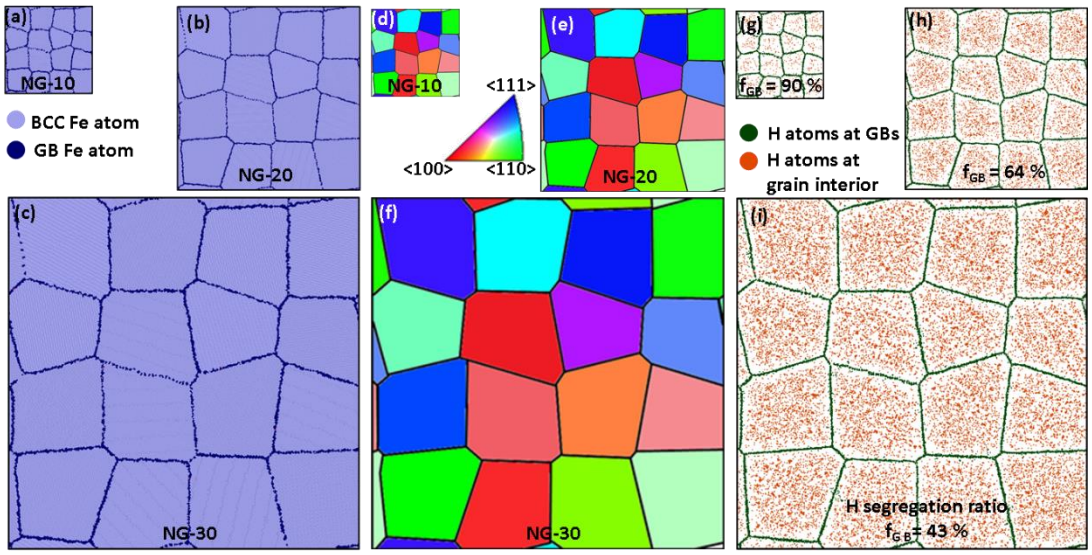

Fig. 1 (a-c) Atomic structures of the NG-10, NG-20, and NG-30 models. The body-centered cubic (BCC) Fe atoms are shown in purple, whereas the GB Fe atoms are shown in navy blue. (d-f) Grain orientations in the NG-10, NG-20, and NG-30 models. (g-i) Distribution of H atoms in the NG-10, NG-20, and NG-30 models. The H atoms at the GBs are shown in dark green, whereas those in the interior of the grains are shown in orange. The GB segregation ratios of H atoms (f_{GB}) for the NG-10, NG-20, and NG-30 models are 90%, 64%, and 43%, respectively.

3. Results

3.1 H diffusion and segregation in the NG α-Fe models

As shown in Fig. 1d-f, large fractions of H atoms are segregated to the GBs after the diffusion simulation. The GB segregation ratio (f_{GB}), which is defined as the number of H atoms located at GBs over the total number of H atoms, for the NG-10, NG-20, and NG-30 models at 300 K is 90 %, 64 %, and 43 %, respectively. Due to the high-density GBs, the effective diffusion coefficient of H in the NG models differs from that of the bulk material. The effective diffusion coefficient of H in the NG models can be expressed as

$$D_{eff} = f_{GB} D_{GB} + f_L D_{bulk} \quad (2)$$

where f_{GB} is the GB segregation ratio; f_L is the fraction of H atoms that are located at lattice sites, which is equal to $1 - f_{GB}$; and D_{GB} and D_{bulk} are the diffusion coefficients of H atoms at the GBs and in the bulk material, respectively[48]. D_{eff} can be derived from the first derivative of the mean square displacement (MSD) of the H atoms as a function of the diffusion time. By calculating the D_{eff} of H atoms in the NG-10, NG-20, and NG-30 models and the bulk Fe and performing linear fitting using Eq. 2, we can derive the value of D_{GB}. The D_{eff} versus f_{GB} relations of H atoms in the NG models and bulk Fe at various temperatures are plotted in Fig. 2a. D_{bulk} at different temperatures are also displayed in Fig. 2a with $f_{GB} = 0$. Note that the D_{eff} of the NG models are lower than D_{bulk}, indicating that the GBs are strong traps for H atoms that will slow rather than accelerate H diffusion.

The derived D_{GB} values at various temperatures are plotted in Fig. 2c. The D_{bulk} values are plotted in Fig. 2b for comparison. By fitting the diffusion coefficient versus temperature relation using the Arrhenius equation, we can determine the diffusion activation energy of the GBs and the bulk material. Fig. 2b shows that within the temperature range from 300 K to 800 K, bulk diffusion has only one activation energy of 0.0374 eV. However, GB diffusion has two activation energies, one at lower temperatures (T < 600 K) and one at higher temperatures (T $\geq$ 600 K), as shown in Fig. 2c. The low-temperature activation energy is 0.0629 eV, whereas the high-temperature activation energy is 0.1089 eV. The increase in the activation energy of GB diffusion indicates a mechanism transition with increasing temperature. We surmise that the increased activation energy at higher temperatures comes from the contribution of Fe atoms that diffuse along the GBs. At higher temperatures, GB self-diffusion is activated, and some H atoms at GBs can diffuse with their neighboring Fe atoms, whereas at a lower temperature, the GB diffusion of Fe atoms is too slow to contribute to the diffusion of H atoms.

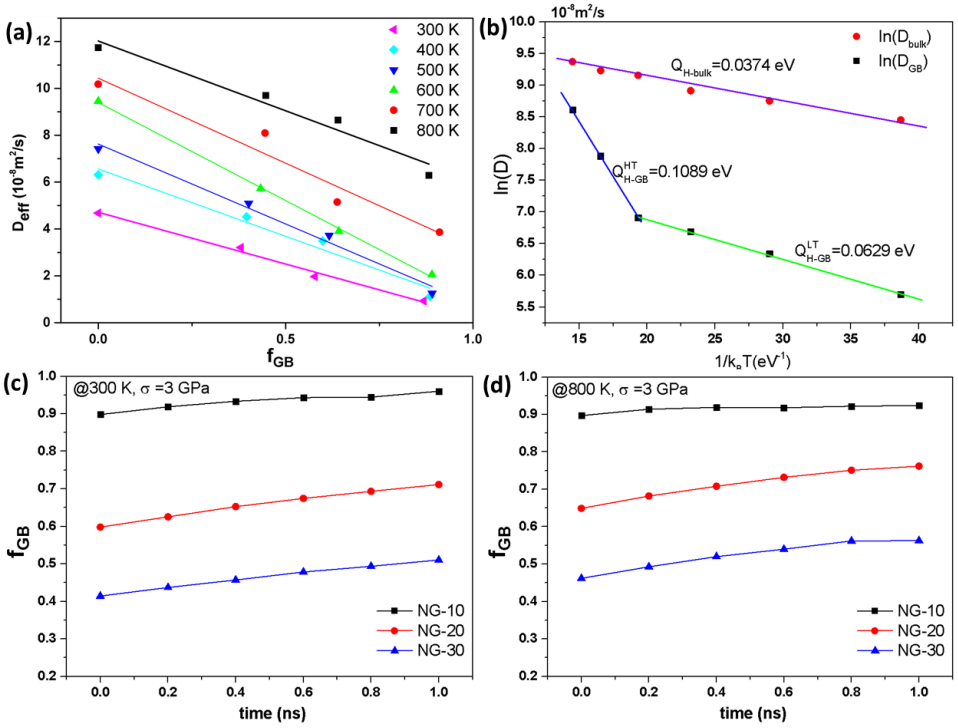

Fig. 2. (a) Effective diffusion coefficient of H in the NG-10, NG-20, and NG-30 models at different temperatures versus GB segregation ratio of H atoms. (b) Arrhenius plot of the H diffusion coefficient of bulk Fe (D_{bulk}) and GBs (D_{GB}). Evolution of the GB segregation ratio of H atoms at (c) 300 K and (d) 800 K under a sustained stress of 3 GPa.

Fig. 2c-d shows the GB segregation ratio versus time during the creep tests of the NG models performed at 300 K and 800 K under a sustained stress of 3 GPa. At this stress level, the H-charged NG models did not exhibit any obvious plastic deformation. Before the creep tests, the H diffusion simulation was performed for 0.5 ns, and the H segregation had already reached equilibrium. However, due to the applied stress, the segregation ratio of the H atoms in the NG models further increased over time during the creep tests. The increase in the H segregation ratio induced by sustained stress was more pronounced in NG-20 and NG-30 than in NG-10. This is because the high H segregation ratio in NG-10 left fewer H atoms in the interior of the grains, whereas in NG-20 and NG-30, there were still many H atoms in the interior of the grains. As the

H atoms diffuse much faster at high temperatures, the H segregation reached equilibrium shortly after the application of sustained stress at 800 K, and the segregation ratio remained approximately constant. However, at 300 K, it took longer for H segregation to reach equilibrium. The increase in the H segregation ratio during the creep tests implies that the sustained stress, which caused more H atoms to accumulate at GBs, should be a crucial factor for the HE of NG materials.

3.2. Creep deformation of the NG α-Fe models

The creep curves of NG-10 at different temperatures and applied stress levels are shown in Fig. 3. The creep curves of NG-20 and NG-30 are shown in S1 and S2 in the Appendix. Some of the creep curves have a typical three-stage structure comprising the primary (transient) creep stage, the secondary (steady) creep stage and the tertiary (rapid acceleration) creep stage; some have only the primary and secondary stages due to the time limitations of the MD simulations. At high temperatures and high applied stress levels, the second stage can be very short, and the model ruptures in a short time. The steady-state creep rates ($\dot{\varepsilon}$), which are determined from the strain rate in the secondary stage, are obtained for the NG models at various temperatures and stress levels.

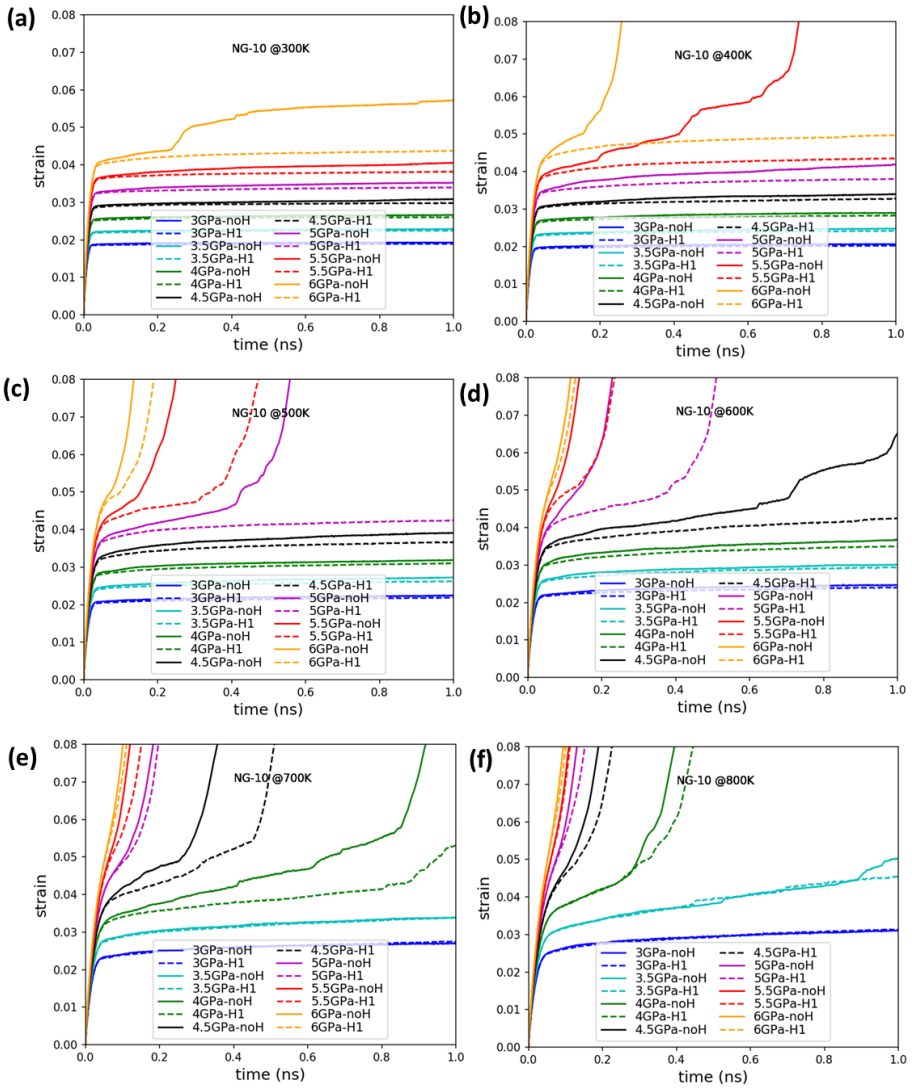

Fig. 3. Creep curves of NG-10 at different temperatures and sustained stress levels.

3.3 Influence of temperature on creep deformation

The logarithmic creep strain rates ($\ln \dot{\varepsilon}$) of the H-charged and uncharged NG-10, NG-20, and NG-30 models at various temperatures and stress levels are plotted against the reciprocal of temperature ($\frac{1}{k_B T}$) in Fig. 4 to illustrate the influence of temperature on the creep strain rate. Fig. 4 indicates that at constant stress and within a certain temperature range, $\ln \dot{\varepsilon}$ has a linear dependence on $\frac{1}{k_B T}$, wherein the slope is the creep activation energy, ΔQ. Noticeably, at low-stress levels, the linear relation

between $\ln \dot{\varepsilon}$ and $\frac{1}{k_B T}$ applies within the temperature range from 300 K to 600 K, wherein the slopes have little difference. At higher stress levels, the linear relation also applies at higher temperatures (600 K to 800 K), but the ΔQ values are largely different. It is found that for each NG model, the transition of ΔQ occurs at a critical logarithmic strain rate ($\ln \dot{\varepsilon}_0$). The values of $\ln \dot{\varepsilon}_0$ of each NG model are slightly different and are shown by the dashed lines in Fig. 4. Accordingly, we can define a low strain rate region (LSRR) that has a strain rate lower than $\dot{\varepsilon}_0$ and a high strain rate region (HSRR) that has a strain rate higher than $\dot{\varepsilon}_0$. In Yang et al.'s work, the stress range was divided into a low-stress region, a medium stress region, and a high-stress region according to different critical sustained stress levels[30]. The ΔQ at each region was obtained subsequently. Since the studied temperatures were within a limited range (25° ~ 70°), the deformation transition mechanism with the increase of temperature was not fully discussed. Herein, the studied temperature range for the creep test is much wider, and the transition mechanisms are observed as the temperature increases. Hereafter, we proposed a new criterion, the critical strain rate $\dot{\varepsilon}_0$, to reveal the deformation mechanism. This adopted criterion considers both the temperature and stress contribution on the deformation and is applicable for creep tests conducted with a wider temperature and stress range.

Fig. 4 also indicates that even within the same region, the ΔQ at different stress levels differs from each other. However, the difference between the ΔQ is quite small within the same region. Since the main objective here is to determine a general ΔQ for LSRR and HSRR, and to reveal the influence of H charging on the creep behavior of NGs, we assume that the ΔQ is independent of σ within LSRR or HSRR. By taking the average of the ΔQ values fitted from the $\ln \dot{\varepsilon}$ of the NG models at different sustained stresses, we determined two ΔQ values from Fig. 4: the creep activation energy at LSRR (denoted ΔQ_{L}) and that at HSRR (denoted ΔQ_{H}). The determined values of ΔQ_{L} and ΔQ_{H} are listed in Table 1.

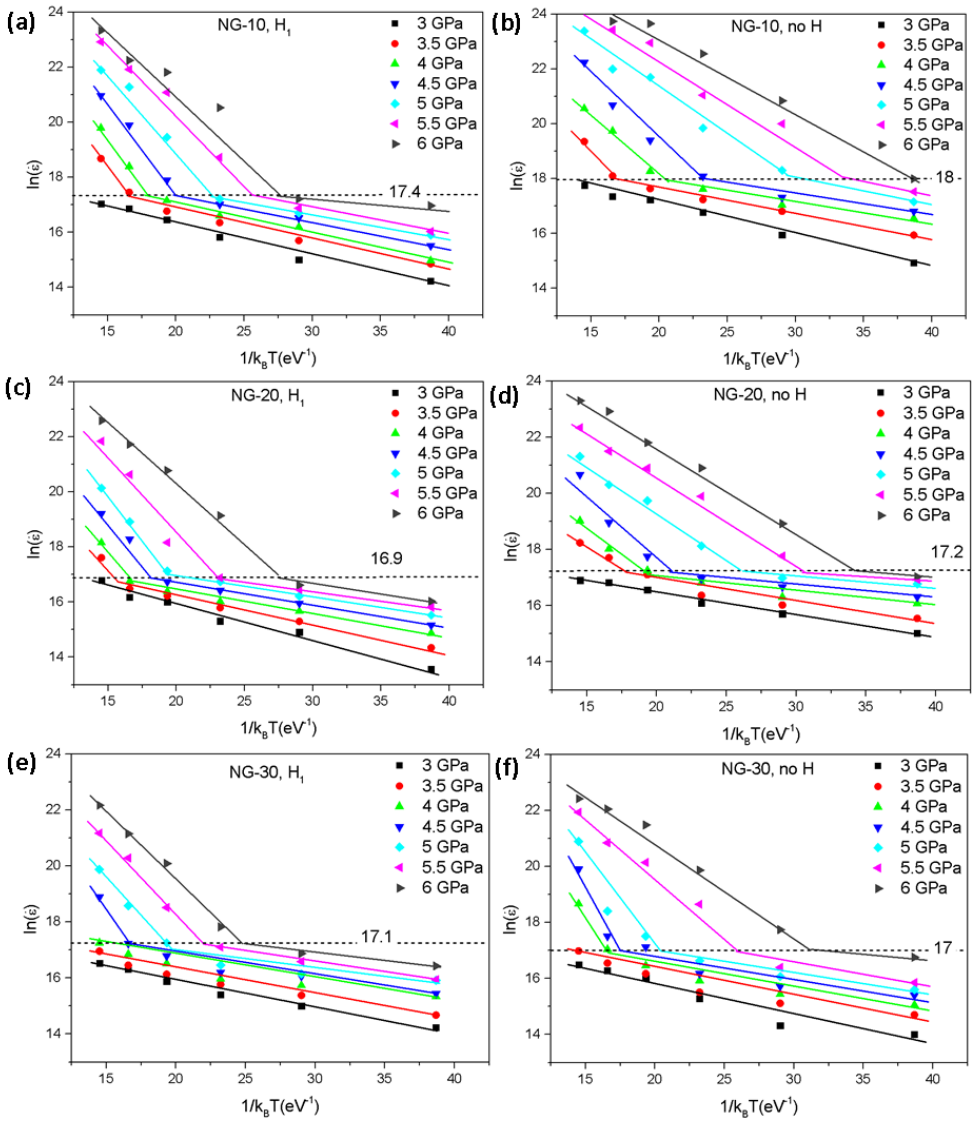

Fig. 4. Logarithmic creep strain rates ($\ln \dot{\varepsilon}$) of the H-charged and uncharged NG-10, NG-20, and NG-30 models at various temperatures and stress levels plotted against the reciprocal of temperature ($\frac{1}{k_B T}$). The logarithmic critical strain rates ($\ln \dot{\varepsilon}_0$) correspond to the transition of the creep mechanism are denoted by the dashed lines.

3.4 Influence of sustained stress on creep deformation

Fig. 5 illustrates $\ln \dot{\varepsilon}$ of the H-charged and uncharged NG-10, NG-20, and NG-30 models at various temperatures and stress levels versus $\ln \sigma$. Fig. 5 indicates that at a constant temperature and within a certain stress range, $\ln \dot{\varepsilon}$ should have a linear dependence on $\ln \sigma$, for which the slope is the stress exponent (n). From the slope

change of the fitted curves, we can also determine a critical strain rate $\dot{\varepsilon}_0$ that corresponds to a sudden change of n. n is a temperature-dependent creep deformation parameter[30]. However, as can be seen from Fig. 5, in the same region, the differences in n at different temperatures are quite small. Here we still assume that within LSRR or HSRR, the n can be regarded as independent of temperature. Based on the same $\dot{\varepsilon}_0$, we can determine the n of each NG model at the LSRR and the HSRR by taking the average of the n values at different temperatures, which are denoted as n_L and n_H, respectively. The values of n_L and n_H of the H-charged and uncharged NG models are listed in Table 1.

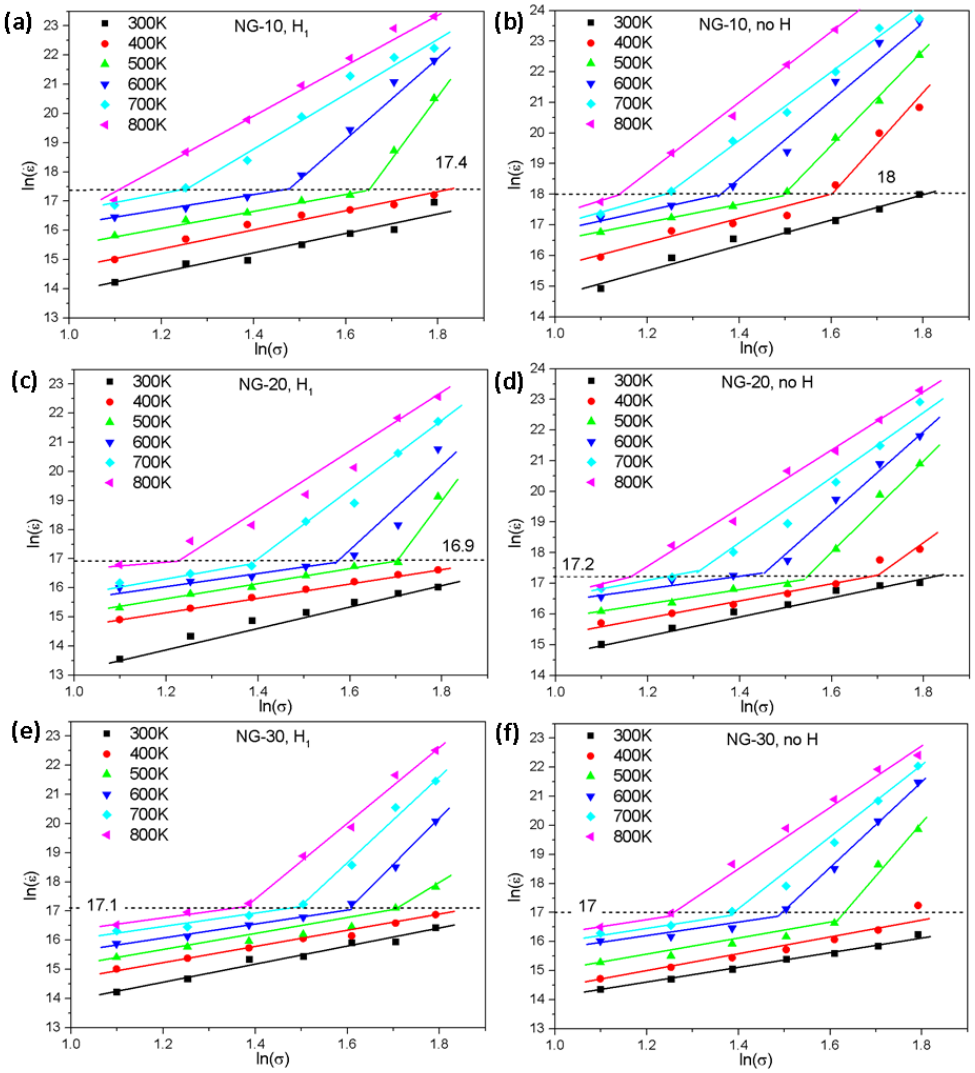

Fig. 5. Logarithmic creep strain rates (ln $\dot{\varepsilon}$) of the H-charged and uncharged NG-10, NG-20, and NG-30 models at various temperatures and stress levels plotted against

$\ln\sigma$. The logarithmic critical strain rates ($\ln\dot{\varepsilon}_0$) correspond to the transition of the creep mechanism are denoted by the dashed lines.

Table 1. Creep deformation parameters

	ΔQ_{L} **(eV)**	n_L	ΔQ_{H} **(eV)**	n_{H}
NG-10-H$_1$	0.1095	3.181333	0.365895	11.075
NG-10-no H	0.096787	3.707333	0.276833	9.48115
NG-20-H$_1$	0.09165	2.730698	0.567768	16.25663
NG-20-no H	0.052408	2.658093	0.379665	12.95068
NG-30-H$_1$	0.068935	2.500775	0.481753	13.09944
NG-30-no H	0.05282	2.59137	0.328	12.17944

3.5 Effect of grain size on creep strain rate

Eq. 1 indicates that at a certain temperature and stress level, plotting $\ln\dot{\varepsilon}$ as functions of $\ln(1/d)$, the grain size exponent (p) can be determined from the slopes. Therefore, there is one p value for each temperature and sustained stress. As there are only 3 grain sizes in our simulations, the determined p values have relatively large deviations. However, we can still obtain the general trend of how the grain size exponent changes with respect to H charging, temperature, and sustained stress. From the p values listed in Table 2, we can see that H charging substantially reduced the p values. Moreover, as temperature and stress increase, the p value generally increases at first and then decreases when the temperature exceeds 700 K and the stress exceeds 5 GPa. The highest p value for the H-charged NG models is 2.57, whereas, for the uncharged NG models, the highest p value is 3.70.

Table 2. Grain size exponent *p* at different temperatures and stress levels

	300 K		400 K		500 K		600 K		700 K		800 K	
σ (GPa)	H_1	no H	H_1	no H	H_1	no H	H_1	no H	H_1	no H	H_1	no H
3	0.10	0.45	0.10	1.03	0.41	1.31	0.54	1.08	0.54	0.88	0.98	1.20
3.5	0.23	1.06	0.32	1.50	0.55	1.54	0.61	1.67	0.96	1.82	1.57	2.10
4	0.29	1.29	0.45	1.42	0.61	1.50	0.63	1.93	1.50	2.46	2.30	1.77
4.5	0.10	1.22	0.45	1.39	0.75	1.73	1.09	2.10	2.41	2.84	1.96	2.14
5	0.05	1.32	0.53	2.02	0.69	2.87	2.15	3.70	2.57	3.18	1.92	2.34
5.5	0.11	1.45	0.30	3.27	1.61	2.12	2.53	2.60	1.31	2.40	1.19	1.58
6	0.20	1.09	0.37	2.94	2.42	2.44	1.56	2.05	0.72	1.50	0.77	1.28

4 Discussion

4.1 Deformation parameters

The values of the creep activation energy ΔQ and the stress exponent *n* at the LSRR and HSRR are listed in Table 1, and the values of the grain size exponent *p* are listed in Table 2. These creep deformation parameters are important indicators of the plastic deformation mechanisms during the creep tests. The transition of ΔQ and *n* suggests that the plastic deformation mechanism changes as the temperature and stress transfer from the LSRR to the HSRR. Comparing the ΔQ of the H-charged and uncharged cases, we can see that H charging can increase ΔQ, and the influence of H charging is more substantial for ΔQ_2. The creep activation energy represents the energy barrier for activating the corresponding plastic deformation mechanism. The higher the activation energy, the more difficult it should be for the mechanism to be activated. The increase of ΔQ_{H} upon H charging demonstrates that H can inhibit dislocation activities at HSRR, which is in accordance with some recent experimental and theoretical observations[49, 50].

Studies have suggested that a stress exponent *n* value of approximately 2 indicates the GB sliding dominated mechanism[51], whereas $n > 4$ indicates the dislocation glide or climb dominated mechanism[29]. The *n* values for the LSRR, n_L, are approximately 3, suggesting that GB sliding might be the deformation mechanism,

whereas those for the HSRR are all higher than 9, indicating that dislocation activities have dominated the plastic deformation. H charging has an obvious effect on the n_H values, which may be attributed to the enhancing effect of H atoms on the dislocation mobility.

The deformation mechanisms can also be inferred from the grain size exponent *p*. For high-temperature (T $\geq$ 600 K) creep, a *p* value of approximately 2 indicates a lattice diffusion deformation mechanism[52], whereas a *p* value of approximately 3 indicates GB diffusion[33]. Table 2 shows that at low-stress levels, as the temperature increases, the *p* values increase in general, indicating that at higher temperatures, the GB movement becomes more dominant. If the *p* value is close to 0, then the deformation mechanism is likely to be dominated by dislocation activity. It is difficult for GB and lattice diffusion to occur at low temperatures; hence, the *p* values are typically less than 2. The reduction in *p* values from H charging indicates that H charging can reduce the diffusion-related creep mechanisms, which might result from the H segregation at GBs.

From the deformation parameters, we can speculate the corresponding mechanism. However, to confirm the mechanisms, we need to investigate the microstructure evolution of the NG models during the creep tests. As the plastic deformation mechanism is highly dependent on temperature and stress, we selected 3 combinations of temperature and stress to reveal the microstructure evolution for mechanism analysis. The combination of 700 K and 3.5 GPa was selected to represent high temperature and low stress, 300 K and 6 GPa represent low temperature and high stress, and 600 K and 5.5 GPa represent high temperature and high stress.

4.2 Deformation mechanism at low stress and high temperature

Fig. 6 displays the defect structures of the NG-10, NG-20, and NG-30 models at 700 K and 3.5 GPa. The Fe atoms with BCC structures are removed to reveal the GB structures and point defects. The frames at the beginning and end of the creep

simulations are plotted, and the two frames are overlapped to demonstrate the changes in the GB structure. The first frame is stretched to have the same length as the last frame and is overlapping the last frame. The combination of 700 K and 3.5 GPa falls into the LSRR for all NG models. Therefore, within the simulation time of 1 ns, the GB structures only changed slightly, which can be seen from the overlapped frames on the rightmost side. GB movement, which involves GB rotation and GB sliding, is the most obvious in the NG-10 models. A comparison of the GB movement in the H-charged and uncharged NG-10 models shows that the segregation of H atoms at GBs can impede GB sliding but not GB rotation. The comparison of the H-charged and uncharged NG-20 and NG-30 models further shows the inhibition of H segregation on the GB movement. The H-charged NG models have nearly no change in GB structure, whereas the uncharged NG models have some obvious GB movements, as indicated by the red circles.

A comparison of the first and last frames of the H-charged NG models also shows that more H atoms segregate to the GBs as the creep simulation elapses, which agrees with the results in Fig. 2c-d. At the end of the creep simulation, additional interstitial Fe atoms and Fe vacancies are also observed inside the grains. This indicates increased lattice diffusion as the creep simulation elapses. The changes in the defect structure through the creep simulation along with the deformation parameters have shown that GB movements and lattice diffusion are the dominant plastic deformation mechanisms. The inhibitory effect of H segregation on the GB movement can be explained by the ‘solute drag effect’[50, 53] of the segregated H atoms. It is well documented that alloying element segregated to the GBs can impede GB movement, due to the reduced GB excess energy by segregation. In this simulation, high fractions of H atoms have segregated on the GBs, thus to the solute drag effect, the segregated H atoms can stabilize the GBs and inhibit GB movement.

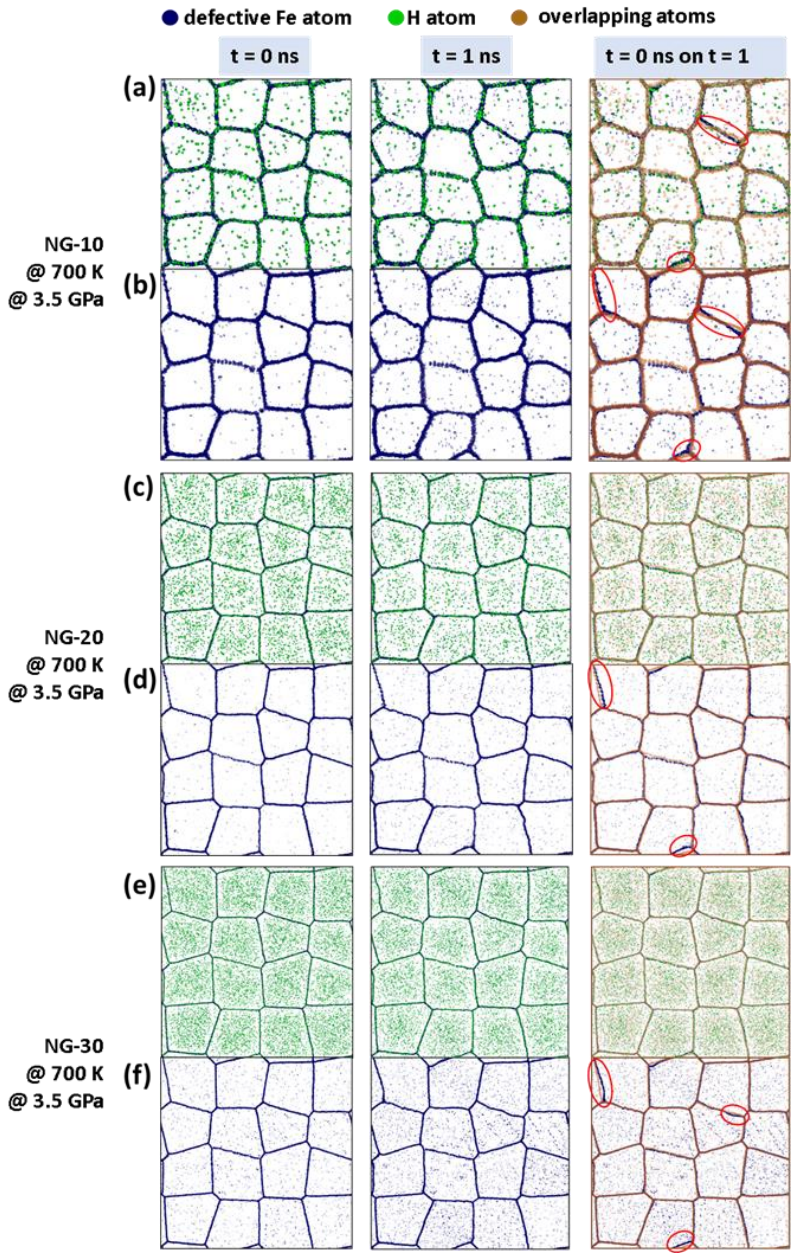

Fig. 6. Defect structures of the first and last frames of the creep simulation of the H-charged and uncharged (a-b) NG-10, (c-d) NG-20, and (e-f) NG-30 models at 700 K and 3.5 GPa. The first frame is stretched to the same length as the last frame and is overlapping the last frame. GBs that have obvious structural changes are circled to show the GB movements.

Since the GB movement plays a crucial role in the creep deformation process, H charging actually increases the creep resistance of the NG models at high

temperatures and low stress. Table 1 shows that the creep activation energy, ΔQ, of the H-charged NG models is higher than that of the corresponding uncharged NG model, indicating that H charging increases the barrier for GB diffusion.

The extents of GB movement in the NG-10, NG-20, and NG-30 models are different, wherein the GBs of NG-10 deform the most and the GBs of NG-30 deform the least. As the fraction of GBs in NG-10 is the highest, the GB-related deformation mechanism in NG-10 participates the most in the plastic deformation process.

In summary, at 700 K and 3.5 GPa, the dominant plastic deformation mechanisms are GB movement and lattice diffusion. GB movement is dominant in the simulation with small grain sizes, owing to their higher fraction of GBs. This result is consistent with many experimental findings that creep deformation in NG metals exhibits a considerable size effect[30, 31, 54, 55]. Since H segregation at GBs has an inhibitory effect on GB movement, GB movement is not as important in the H-charged NG models as in the uncharged NG models. Due to the inhibition of H atoms on the GB movement, the H-charged NG models seem to have higher creep resistance at 700 K and 3.5 GPa.

4.3 Deformation mechanism at high stress and low temperature

The temperature and stress in Fig. 7 are 300 K and 6 GPa, respectively, which still lies in the LSRR for all the NG models. For NG-10 and uncharged NG-20 and NG-30, the strain rates are very close to the critical strain rate; hence, the plastic deformation has changed to dislocation and DT nucleation. DT formation is an important deformation mechanism of BCC metals. The formation of DTs usually becomes more difficult as the grain size decreases. However, when the grain size reaches the nanometer scale, DTs are frequently observed[56, 57]. In this simulation, the grain sizes of the NG models are favorable for DT formation; hence, DT activities played an important role during the creep process of the NG models. As shown in Fig. 7, dislocations and DTs are all emitted from the GBs. The dislocations propagate and

vanish at the GBs as the creep simulation elapses (see Fig. 7b, Fig. 7d, and Fig. 7f).

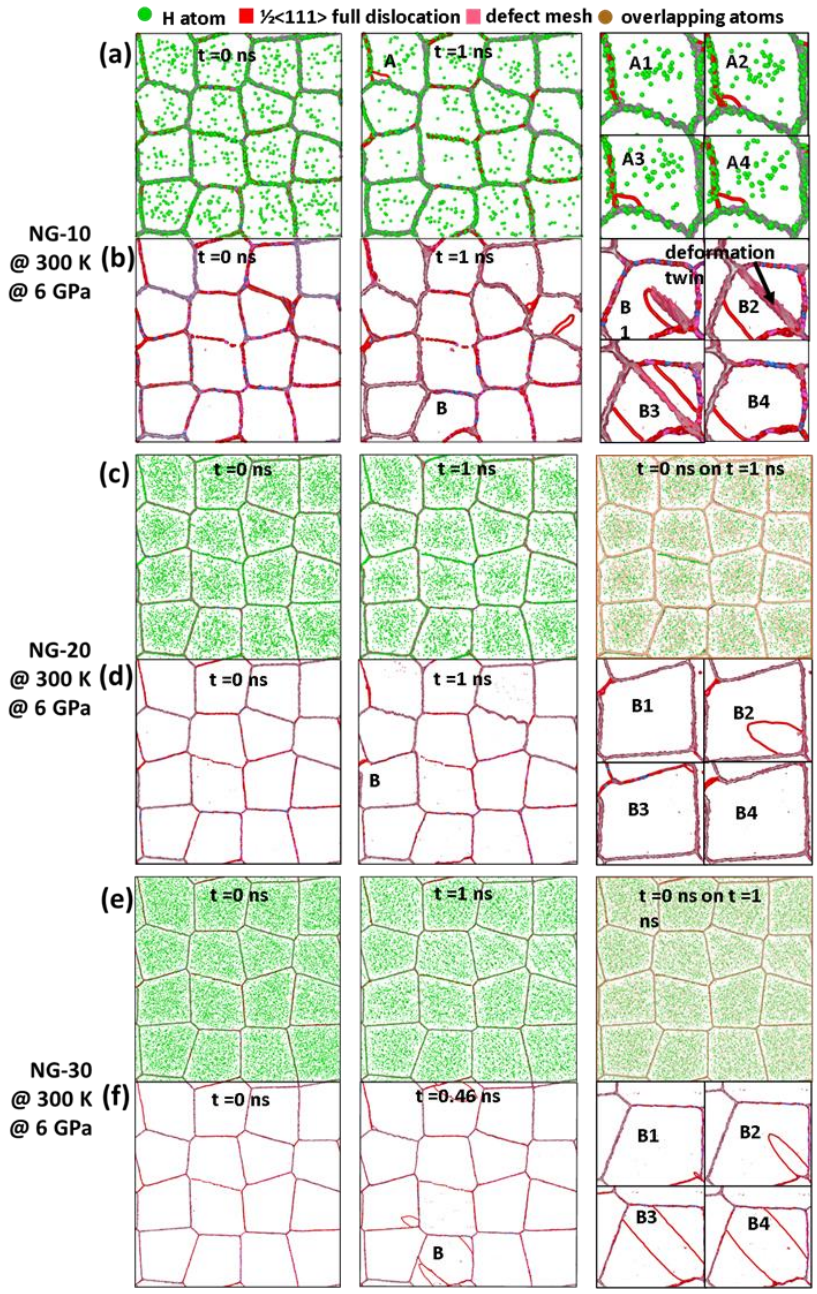

Fig. 7. Defect structures of the first and last frames of the creep simulation of the H-charged and uncharged (a-b) NG-10, (c-d) NG-20, and (e-f) NG-30 models at 300 K and 6 GPa. The defect mesh and dislocations are visualized by DXA. For the NG models that have no dislocation nucleation, the first and last frames are overlapped to reveal the changes in the GB structures; for those having dislocation and DT nucleation, the nucleation and propagation processes are shown in the rightmost plots.

No dislocation or DT activities are found in the H-charged NG-20 and NG-30 models (Fig. 7c and Fig. 7e), which might be attributed to the inhibitory effect of H charging on dislocation and DT nucleation. Although dislocation nucleation was observed at the GBs of H-charged NG-10, it did not propagate into the interior of the grains due to the lack of a driving force (Fig. 7a). The inhibitory effect of H segregation on the nucleation of dislocations and DTs from GBs makes lattice diffusion the deformation mechanism for the H-charged NG-20 and NG-30 at low temperature and high stress.

The influence of H charging on dislocation nucleation is a controversial issue. The well-known hydrogen enhanced local plasticity (HELP) theory[17] suggests that H can reduce the dislocation nucleation and movement barrier, thereby softening the material. However, recent experimental and theoretical investigations have challenged the HELP theory. The MD simulation conducted by Song and Curtin[49] suggests that H atoms reduce dislocation mobility. Creep tests performed by Matsunaga et al. on Zircaloy-4 indicate that the creep rate was reduced by H charging and dislocation activities were reduced by H atoms. Transmission electron microscopy observation suggested that the H atmosphere had a dragging effect on the dislocation activities and suppressed the cross-slip process during the creep tests[50]. In the current work, H charging is found to have an inhibitory effect on dislocation nucleation from the GBs. We suppose that the solute drag effect induced by the H atoms segregated causes the inhibition of dislocation nucleation. The nucleation of dislocations usually initiates at a ledge on the GBs[43, 58, 59]. However, the segregated H atoms have limited the movement of GB atoms, and subsequently limited the ledge formation and dislocation nucleation.

In summary, at 300 K and 6 GPa, as the strain rates of the NG models are very close to the critical strain rate, a transition in the deformation mechanism is likely to occur. However, due to the inhibitory effect of H charging, the H-charged NG models did not sustain obvious plastic deformation within the duration of the simulation.

Combining the results in Figs. 6 and 7, we find that H charging has an inhibitory effect on GB-related deformations such as GB sliding and dislocation nucleation at GBs.

4.4 Deformation mechanism at high stress and high temperature

The defect structure evolution during the creep simulation of the H-charged and uncharged NG-10, NG-20, and NG-30 models at 600 K and 5.5 GPa is shown in Fig. 8. At this temperature and stress, all the NG models had a large degree of plastic deformation at the end of the creep simulations, in which the dislocation and DT activities were the dominant deformation mechanism. Most of the NG models fractured before the end of the simulation, as shown in the creep strain versus time curves plotted in Figs. 3, A1, and A2. The microstructures of the H-charged and uncharged models with the same strains are compared. The H-charged NG models had GB fractures at lower strains than the uncharged models. The fractured GBs of the H-charged models also had much flatter surfaces than those of the uncharged models, indicating that GB decohesion was induced by H segregation. The inhibition of dislocation and DT nucleation by H charging can also be observed. At a strain of 0.063, the H-charged models had much less dislocation and DT nucleation than the uncharged models. However, at high strain levels, there were large numbers of dislocations and DTs in both H-charged and uncharged models. The main HE mechanism in the NG models was the hydrogen-enhanced decohesion mechanism. Although H charging substantially reduced the ductility of the NG models, plastic deformation still occurred before the GB fracture. This finding is in accordance with the experimental observations of slip bands near the intergranular crack surface of the hydrogen embrittled samples[60].

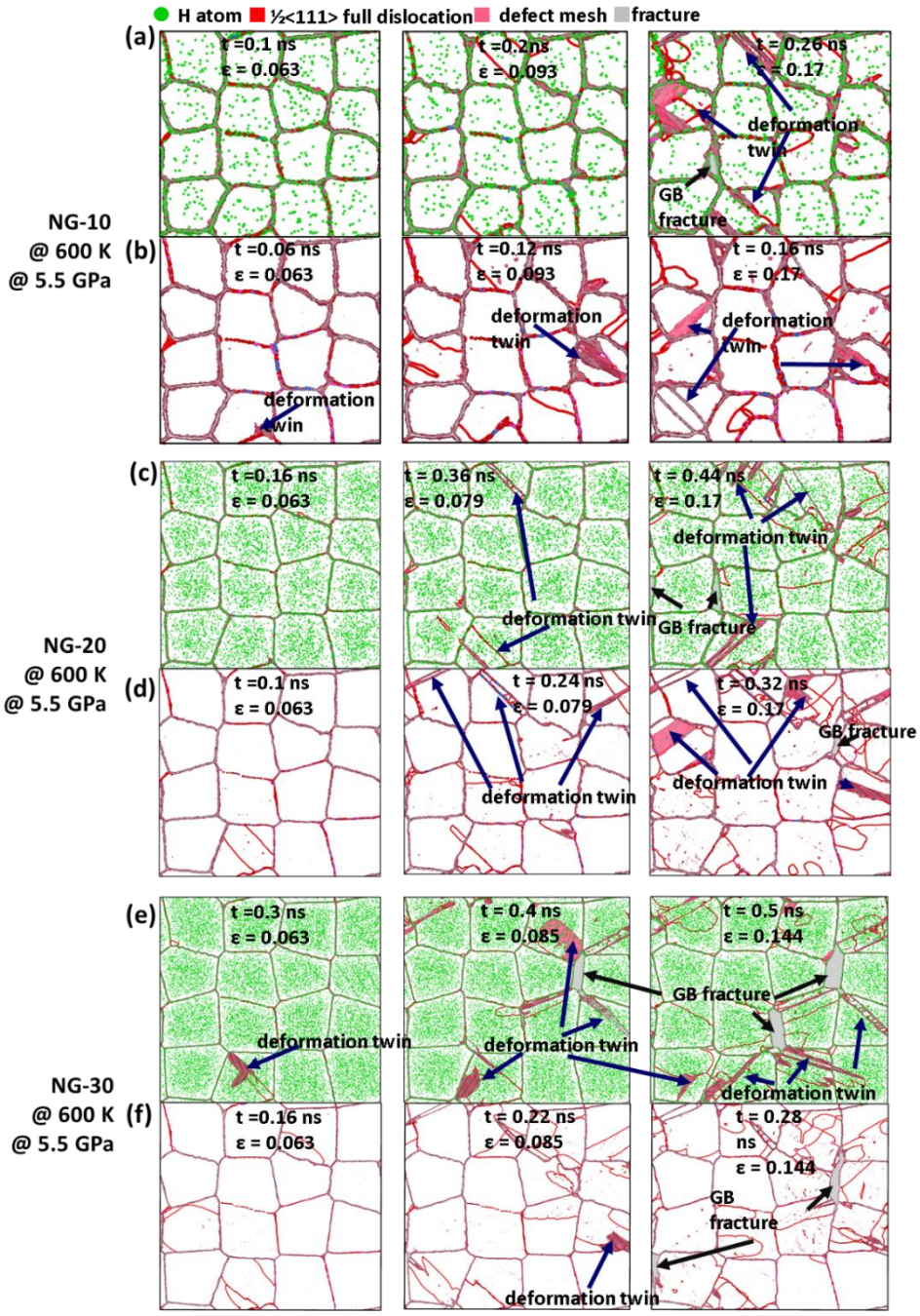

Fig. 8. Defect structure evolution during the creep simulation of the H-charged and uncharged (a-b) NG-10, (c-d) NG-20, and (e-f) NG-30 models at 600 K and 5.5 GPa. The defect mesh and dislocations are calculated and visualized by DXA.

As the fraction of GBs was the highest in NG-10, the GBs deformed the most in the NG-10 models. GB movement contributed greatly to the ductility of NG-10. The

uncharged NG-10 had no GB fractures at a strain of 0.17, whereas the uncharged NG-20 and NG-30 both had GB fractures. Even with H charging, NG-10 had only a small void formed at one GB, whereas GB decohesion occurred in the H-charged NG-20 and NG-30 models. H charging had a little inhibitory effect on GB movements, but since the main deformation mechanism was dislocation and DT movement, the inhibitory effect on the GB movement was not obvious.

In summary, at 600 K and 5.5 GPa, the dominant deformation mechanism was dislocation and DT activities. Dislocations and DTs that nucleated at the GBs propagated and vanished at the GBs during creep deformation. Finally, the NG models ruptured by GB fracture. H charging substantially reduced the ductility of the NG models, with hydrogen-enhanced decohesion of GBs being the main HE mechanism. The inhibition of H segregation at GBs on dislocation nucleation was clearly observed. Owing to the high fraction of GBs in NG-10, the H-charged and uncharged NG-10 models both exhibited higher ductility than the NG-20 and NG-30 models.

4.5 Influence of H charging and grain size on the temperature- and stress-dependent plastic deformation mechanisms of the NG models

The microstructure evolutions of the NG models during the creep simulations revealed the plastic deformation mechanisms with atomic-level details. The plastic deformation mechanisms are mainly dependent on temperature and stress. The grain size and H charging also influence the mechanisms. The influence of grain size is mainly manifested in the importance of the GB movement as a deformation mechanism. NG models with smaller grain sizes have a higher fraction of GBs, and subsequently, the GB movement plays a more important role in the plastic deformation process. Owing to this grain size effect, the critical strain rate ($\dot{\varepsilon}_0$) also becomes grain size-dependent, as shown in Fig. 9. This figure displays the contours of the logarithmic strain rate as functions of the logarithmic stress and temperature of the

H-charged and uncharged NG-10, NG-20, and NG-30 models. The critical strain rates separating the HSRR and LSRR are indicated with dashed lines. The $\ln \dot{\varepsilon}_0$ values of the NG-10 models are higher than those of the NG-20 and NG-30 models. As the grain size increases, the dashed lines in Fig. 9 shift upwards, indicating that the NG models with smaller grain sizes have lower creep resistance and require lower temperature and stress to activate dislocation and DT activities.

The influence of H charging is also shown in Fig. 9. The dashed line showing the value of $\ln \dot{\varepsilon}_0$ shifts upwards in response to H charging. As previously stated, H segregation at GBs has an inhibitory effect on GB-related deformation mechanisms, such as GB diffusion and dislocation nucleation. Therefore, with H charging, the onset of dislocation and DT activities requires higher stress or temperature. The changes of ΔQ_H and n_{H} induced by H charging also suggest the inhibitory effect of H atoms on dislocation activities.

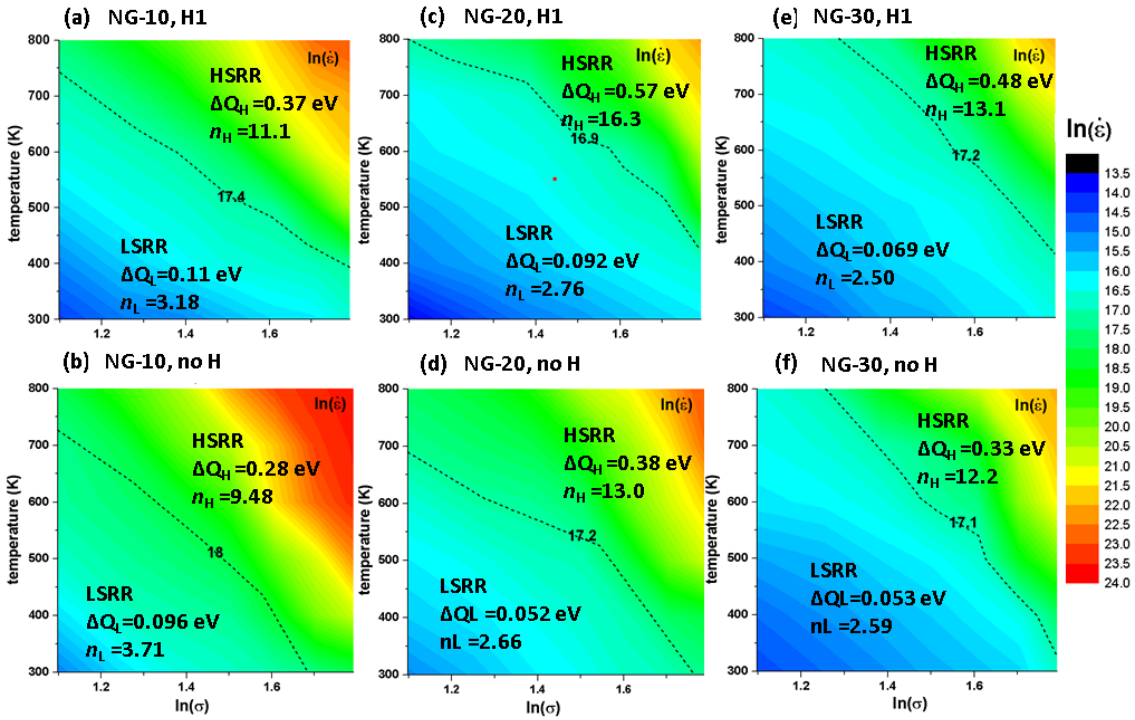

Fig. 9. Contours of the logarithmic strain rate as functions of logarithmic stress and temperature of the H-charged and uncharged NG-10, NG-20, and NG-30 models. The critical strain rates separating the HSRR and LSRR are indicated with dashed lines.

The temperature- and stress-dependent deformation mechanisms of the NG models are summarized in Fig. 10. The dashed lines represent the critical strain rate of the deformation mechanism transition. At the HSRR, the main deformation mechanism is the dislocation and DT activities. As the temperature increases, GB diffusion becomes increasingly important, whereas, at lower temperatures, the deformation is mainly mediated by dislocations and DTs. At the LSRR, the strain rate is much lower; hence, the plastic deformation during the creep simulation is not obvious. At higher temperatures, the deformation mechanism is mostly GB diffusion. At low temperatures and high stress, the deformation mechanism is mainly lattice diffusion; however, when the strain rate is very close to $\dot{\varepsilon}_0$, dislocation and DT nucleation will participate in the deformation process. At the lowest temperatures and stresses, as the strain rate is too low and the simulation time is limited, no obvious plastic deformation occurs during creep deformation.

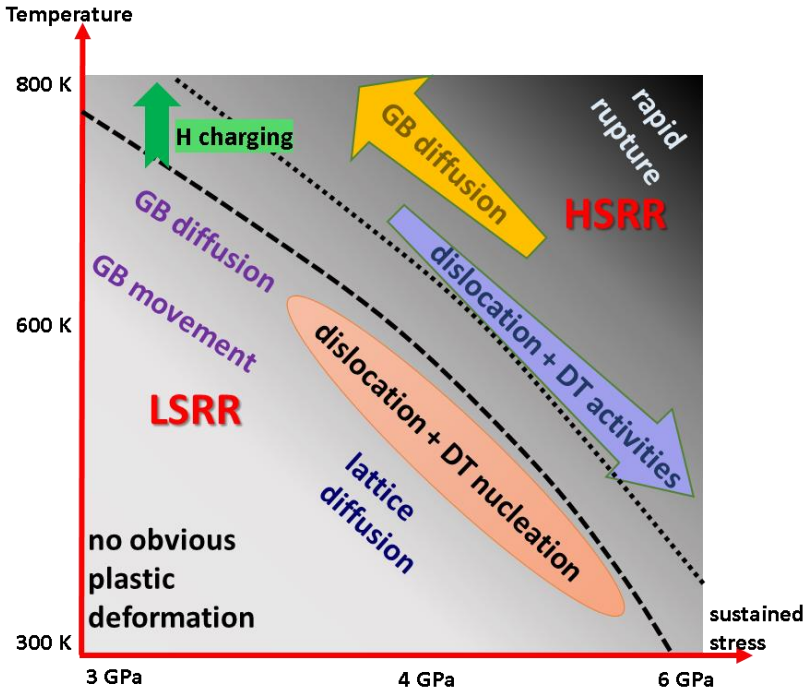

Fig. 10. Temperature- and stress-dependent deformation mechanisms of the NG models. The dashed lines represent the critical strain rate of the deformation mechanism transition.

The influences of H charging on different deformation mechanisms are different. At the HSRR, H segregation at GBs can inhibit dislocation or DT nucleation. The changes in creep activation energy and stress exponent at HSRR induced by H charging also suggest the inhibitory effect of H atoms on dislocation activities. The GB diffusion at a higher temperature will also be inhibited by H charging. Although H charging can delay plastic deformation, the segregated H atoms at GBs will weaken the GB strength, resulting in early GB fractures. Moreover, the inhibition of the GB movement will also reduce the ductility of the NG models, particularly in the NG-10 model where the GB movement plays an important role in the deformation process. At the LSRR, the inhibitory effect of H charging is more pronounced since GB diffusion is the main deformation mechanism. The dashed line representing the critical strain rate will be shifted upwards by H charging.

Finally, we would like to discuss the applicability of the current theoretical work. The current model mainly focuses on the effect of GBs on H diffusion and creep behaviors NGs, hence the effect of other lattice defects such as dislocations and vacancies are ignored. In real metals, dislocations and vacancies always exist. Therefore, the creep behavior and the influence of H on the plastic deformation in real metals should be more complicated. However, in NG metals, where GBs are the main lattice defects and play the dominant role affecting plastic deformation of NGs, the model is applicable.

5 Conclusions

In the present work, the HE behavior and mechanism of NG α-Fe were investigated by performing MD simulations of creep tests of NG α-Fe. As the temperature and stress increased, there was an obvious transition in the deformation parameters, suggesting a change in the plastic deformation mechanism. It was found that H atoms segregated at GBs had an inhibitory effect on GB movement, dislocation, and DT nucleation at GBs. As the grain size increased, the GB-related deformation

modes became less important, and the HE mechanism transitioned from H-induced inhibition of GB-related deformation to H-enhanced GB decohesion. The current results might provide theoretical guidance for designing NG structural materials with low HE sensitivity and better mechanical performance.

Acknowledgments

This research was supported by the Key-Area Research and Development Program of Guangdong Province (2019B111107002), the National Key Research and Development Program of China (2018YFE0124900), the National Natural Science Foundation of China (Nos. 51901013/51861165204/51971187), and the Fundamental Research Funds for the Central Universities (University of Science and Technology Beijing (No. 06500135).

Data availability statement

The processed data required to reproduce these findings are available upon request.

References

[1] M. Dao, L. Lu, R.J. Asaro, J.T.M. De Hosson, E. Ma, Toward a quantitative understanding of mechanical behavior of nanocrystalline metals, Acta Materialia 55(12) (2007) 4041-4065.
[2] L. Sun, X. He, J. Lu, Nanotwinned and hierarchical nanotwinned metals: a review of experimental, computational and theoretical efforts, npj Computational Materials 4(1) (2018) 6.
[3] Z. Shan, E.A. Stach, J.M.K. Wiezorek, J.A. Knapp, D.M. Follstaedt, S.X. Mao, Grain Boundary-Mediated Plasticity in Nanocrystalline Nickel, Science 305(5684) (2004) 654.
[4] J. Schiøtz, F.D. Di Tolla, K.W. Jacobsen, Softening of nanocrystalline metals at very small grain sizes, Nature 391(6667) (1998) 561-563.
[5] J.P. Hirth, Effects of hydrogen on the properties of iron and steel, Metallurgical Transactions A 11(6) (1980) 861-890.
[6] C. Pandey, N. Saini, M.M. Mahapatra, P. Kumar, Hydrogen induced cold cracking

of creep resistant ferritic P91 steel for different diffusible hydrogen levels in deposited metal, International Journal of Hydrogen Energy 41(39) (2016) 17695-17712.
[7] N. Saini, C. Pandey, M.M. Mahapatra, Effect of diffusible hydrogen content on embrittlement of P92 steel, International Journal of Hydrogen Energy 42(27) (2017) 17328-17338.
[8] C. Pandey, M.M. Mahapatra, P. Kumar, N. Saini, Diffusible Hydrogen Level in Deposited Metal and Their Effect on Tensile Properties and Flexural Strength of P91 Steel, J. Eng. Mater. Technol. 139(3) (2017).
[9] C. Pandey, M.M. Mahapatra, P. Kumar, N. Saini, A. Srivastava, Microstructure and mechanical property relationship for different heat treatment and hydrogen level in multi-pass welded P91 steel joint, Journal of Manufacturing Processes 28 (2017) 220-234.
[10] S. Wang, M.L. Martin, I.M. Robertson, P. Sofronis, Effect of hydrogen environment on the separation of Fe grain boundaries, Acta Materialia 107 (2016) 279-288.
[11] A. Oudriss, J. Creus, J. Bouhattate, E. Conforto, C. Berziou, C. Savall, X. Feaugas, Grain size and grain-boundary effects on diffusion and trapping of hydrogen in pure nickel, Acta Materialia 60(19) (2012) 6814-6828.
[12] X.-Y. Zhou, J.-H. Zhu, H.-H. Wu, Molecular dynamics studies of the grain-size dependent hydrogen diffusion coefficient of nanograined Fe, International Journal of Hydrogen Energy (2020).
[13] S. Huang, D. Chen, J. Song, D.L. McDowell, T. Zhu, Hydrogen embrittlement of grain boundaries in nickel: an atomistic study, npj Computational Materials 3(1) (2017) 28.
[14] M. Koyama, C.C. Tasan, E. Akiyama, K. Tsuzaki, D. Raabe, Hydrogen-assisted decohesion and localized plasticity in dual-phase steel, Acta Materialia 70 174-187.
[15] X.-Y. Zhou, X.-S. Yang, J.-H. Zhu, F. Xing, Atomistic simulation study of the grain-size effect on hydrogen embrittlement of nanograined Fe, International Journal of Hydrogen Energy 45(4) (2020) 3294-3306.
[16] L. Chen, X. Xiong, X. Tao, Y. Su, L. Qiao, Effect of dislocation cell walls on hydrogen adsorption, hydrogen trapping and hydrogen embrittlement resistance, Corrosion Science 166 (2020) 108428.
[17] M.L. Martin, M. Dadfarnia, A. Nagao, S. Wang, P. Sofronis, Enumeration of the hydrogen-enhanced localized plasticity mechanism for hydrogen embrittlement in structural materials, Acta Materialia 165 (2019) 734-750.
[18] M. Nagumo, K. Takai, The predominant role of strain-induced vacancies in hydrogen embrittlement of steels: Overview, Acta Materialia 165 (2019) 722-733.
[19] O. Verners, G. Psofogiannakis, A.C.T. van Duin, Comparative molecular dynamics study of fcc-Al hydrogen embrittlement, Corrosion Science 98 (2015) 40-49.
[20] C. Park, N. Kang, S. Liu, Effect of grain size on the resistance to hydrogen embrittlement of API 2W Grade 60 steels using in situ slow-strain-rate testing, Corrosion Science 128 (2017) 33-41.

[21] Y. Bai, Y. Momotani, M.C. Chen, A. Shibata, N. Tsuji, Effect of grain refinement on hydrogen embrittlement behaviors of high-Mn TWIP steel, Materials Science and Engineering: A 651 (2016) 935-944.
[22] S. Chen, M. Zhao, L. Rong, Effect of grain size on the hydrogen embrittlement sensitivity of a precipitation strengthened Fe–Ni based alloy, Materials Science and Engineering: A 594 (2014) 98-102.
[23] A. Macadre, T. Tsuchiyama, S. Takaki, Control of hydrogen-induced failure in metastable austenite by grain size refinement, Materialia 8 (2019) 100514.
[24] M. Koyama, K. Ichii, K. Tsuzaki, Grain refinement effect on hydrogen embrittlement resistance of an equiatomic CoCrFeMnNi high-entropy alloy, International Journal of Hydrogen Energy 44(31) (2019) 17163-17167.
[25] Y. Mine, N. Horita, Z. Horita, K. Takashima, Effect of ultrafine grain refinement on hydrogen embrittlement of metastable austenitic stainless steel, International Journal of Hydrogen Energy 42(22) (2017) 15415-15425.
[26] K. Takasawa, R. Ikeda, N. Ishikawa, R. Ishigaki, Effects of grain size and dislocation density on the susceptibility to high-pressure hydrogen environment embrittlement of high-strength low-alloy steels, International Journal of Hydrogen Energy 37(3) (2012) 2669-2675.
[27] N. Zan, H. Ding, X. Guo, Z. Tang, W. Bleck, Effects of grain size on hydrogen embrittlement in a Fe-22Mn-0.6C TWIP steel, International Journal of Hydrogen Energy 40(33) (2015) 10687-10696.
[28] B. Cai, Q.P. Kong, L. Lu, K. Lu, Low temperature creep of nanocrystalline pure copper, Materials Science and Engineering: A 286(1) (2000) 188-192.
[29] A.M. Brown, M.F. Ashby, On the power-law creep equation, Scripta Metallurgica 14(12) (1980) 1297-1302.
[30] X.-S. Yang, Y.-J. Wang, H.-R. Zhai, G.-Y. Wang, Y.-J. Su, L.H. Dai, S. Ogata, T.-Y. Zhang, Time-, stress-, and temperature-dependent deformation in nanostructured copper: Creep tests and simulations, Journal of the Mechanics and Physics of Solids 94 (2016) 191-206.
[31] X.-S. Yang, H.-R. Zhai, H.-H. Ruan, S.-Q. Shi, T.-Y. Zhang, Multi-temperature indentation creep tests on nanotwinned copper, International Journal of Plasticity 104 (2018) 68-79.
[32] X.-S. Yang, Y.-J. Wang, G.-Y. Wang, H.-R. Zhai, L.H. Dai, T.-Y. Zhang, Time, stress, and temperature-dependent deformation in nanostructured copper: Stress relaxation tests and simulations, Acta Materialia 108 (2016) 252-263.
[33] R.L. Coble, A Model for Boundary Diffusion Controlled Creep in Polycrystalline Materials, J. Appl. Phys. 34(6) (1963) 1679-1682.
[34] J. Song, W. Curtin, Atomic mechanism and prediction of hydrogen embrittlement in iron, Nature materials 12(2) (2013) 145.
[35] X. Zhou, B. Ouyang, W.A. Curtin, J. Song, Atomistic investigation of the influence of hydrogen on dislocation nucleation during nanoindentation in Ni and Pd, Acta Materialia 116 (2016) 364-369.

[36] A. Tehranchi, W.A. Curtin, Atomistic study of hydrogen embrittlement of grain boundaries in nickel: I. Fracture, Journal of the Mechanics and Physics of Solids 101 (2017) 150-165.
[37] X. Xing, W. Chen, H. Zhang, Atomistic study of hydrogen embrittlement during cyclic loading: Quantitative model of hydrogen accumulation effects, International Journal of Hydrogen Energy 42(7) (2017) 4571-4578.
[38] X. Xing, M. Yu, W. Chen, H. Zhang, Atomistic simulation of hydrogen-assisted ductile-to-brittle transition in α-iron, Computational Materials Science 127 (2017) 211-221.
[39] L. Wan, W.T. Geng, A. Ishii, J.-P. Du, Q. Mei, N. Ishikawa, H. Kimizuka, S. Ogata, Hydrogen embrittlement controlled by reaction of dislocation with grain boundary in alpha-iron, International Journal of Plasticity 112 (2019) 206-219.
[40] Y. Zhu, Z. Li, M. Huang, Solute hydrogen effects on plastic deformation mechanisms of α-Fe with twist grain boundary, International Journal of Hydrogen Energy 43(22) (2018) 10481-10495.
[41] J. Schiøtz, Atomic-scale modeling of plastic deformation of nanocrystalline copper, Scripta Materialia 51(8) (2004) 837-841.
[42] T. Zhang, K. Zhou, Z.Q. Chen, Strain rate effect on plastic deformation of nanocrystalline copper investigated by molecular dynamics, Materials Science and Engineering: A 648 (2015) 23-30.
[43] M. Dupraz, Z. Sun, C. Brandl, H. Van Swygenhoven, Dislocation interactions at reduced strain rates in atomistic simulations of nanocrystalline Al, Acta Materialia 144 (2018) 68-79.
[44] A. Ramasubramaniam, M. Itakura, E.A. Carter, Interatomic potentials for hydrogen in α-iron based on density functional theory, Physical Review B 79(17) (2009) 174101.
[45] P. Steve, Fast parallel algorithms for short-range molecular dynamic, Academic Press Professional, Inc.1995.
[46] A. Stukowski, Visualization and analysis of atomistic simulation data with OVITO-the Open Visualization Tool, Modelling & Simulation in Materials Science & Engineering 18(6) (2010) 2154-2162.
[47] J.D. Honeycutt, H.C. Andersen, Molecular dynamics study of melting and freezing of small Lennard-Jones clusters, The Journal of Physical Chemistry 91(19) (1987) 4950-4963.
[48] J.B. Leblond, D. Dubois, A general mathematical description of hydrogen diffusion in steels—II. Numerical study of permeation and determination of trapping parameters, Acta Metallurgica 31(10) (1983) 1471-1478.
[49] J. Song, W.A. Curtin, Mechanisms of hydrogen-enhanced localized plasticity: An atomistic study using α-Fe as a model system, Acta Materialia 68 (2014) 61-69.
[50] T. Matsunaga, H. Hongo, M. Tabuchi, Y. Satoh, H. Abe, Transition of creep mechanism by solute hydrogen in Zircaloy-4, Materials Science and Engineering: A 684 (2017) 191-195.

[51] H. Lüthy, R.A. White, O.D. Sherby, Grain boundary sliding and deformation mechanism maps, Materials Science and Engineering 39(2) (1979) 211-216.
[52] C. Herring, Diffusional Viscosity of a Polycrystalline Solid, J. Appl. Phys. 21(5) (1950) 437-445.
[53] G. Miyamoto, K. Yokoyama, T. Furuhara, Quantitative analysis of Mo solute drag effect on ferrite and bainite transformations in Fe-0.4C-0.5Mo alloy, Acta Materialia 177 (2019) 187-197.
[54] P. Huang, F. Wang, M. Xu, K.W. Xu, T.J. Lu, Dependence of strain rate sensitivity upon deformed microstructures in nanocrystalline Cu, Acta Materialia 58(15) (2010) 5196-5205.
[55] Z.H. Cao, L. Wang, K. Hu, Y.L. Huang, X.K. Meng, Microstructural evolution and its influence on creep and stress relaxation in nanocrystalline Ni, Acta Materialia 60(19) (2012) 6742-6754.
[56] P.C. Millett, T. Desai, V. Yamakov, D. Wolf, Atomistic simulations of diffusional creep in a nanocrystalline body-centered cubic material, Acta Materialia 56(14) (2008) 3688-3698.
[57] B. Jiang, A. Tu, H. Wang, H. Duan, S. He, H. Ye, K. Du, Direct observation of deformation twinning under stress gradient in body-centered cubic metals, Acta Materialia 155 (2018) 56-68.
[58] Y. Guo, D.M. Collins, E. Tarleton, F. Hofmann, A.J. Wilkinson, T.B. Britton, Dislocation density distribution at slip band-grain boundary intersections, Acta Materialia 182 (2020) 172-183.
[59] X.Y. Sun, C. Fressengeas, V. Taupin, P. Cordier, N. Combe, Disconnections, dislocations and generalized disclinations in grain boundary ledges, International Journal of Plasticity 104 (2018) 134-146.
[60] M.L. Martin, B.P. Somerday, R.O. Ritchie, P. Sofronis, I.M. Robertson, Hydrogen-induced intergranular failure in nickel revisited, Acta Materialia 60(6) (2012) 2739-2745.

Appendix

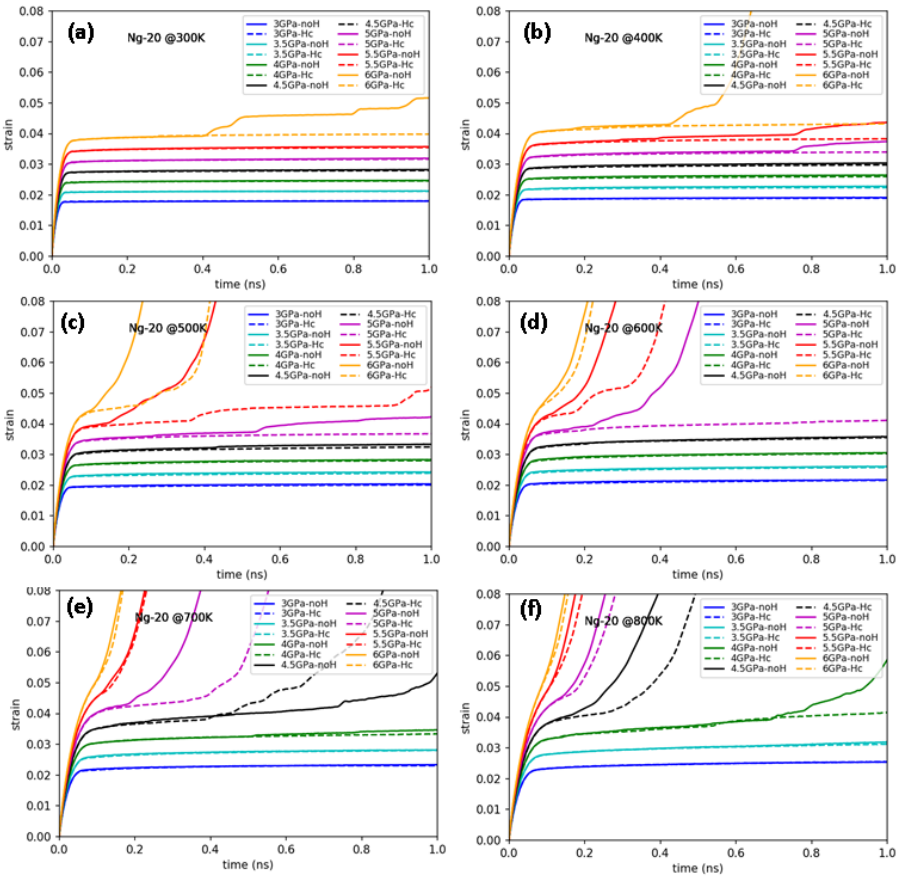

A1. The creep curves of the NG-20 at different temperatures and sustained stress.

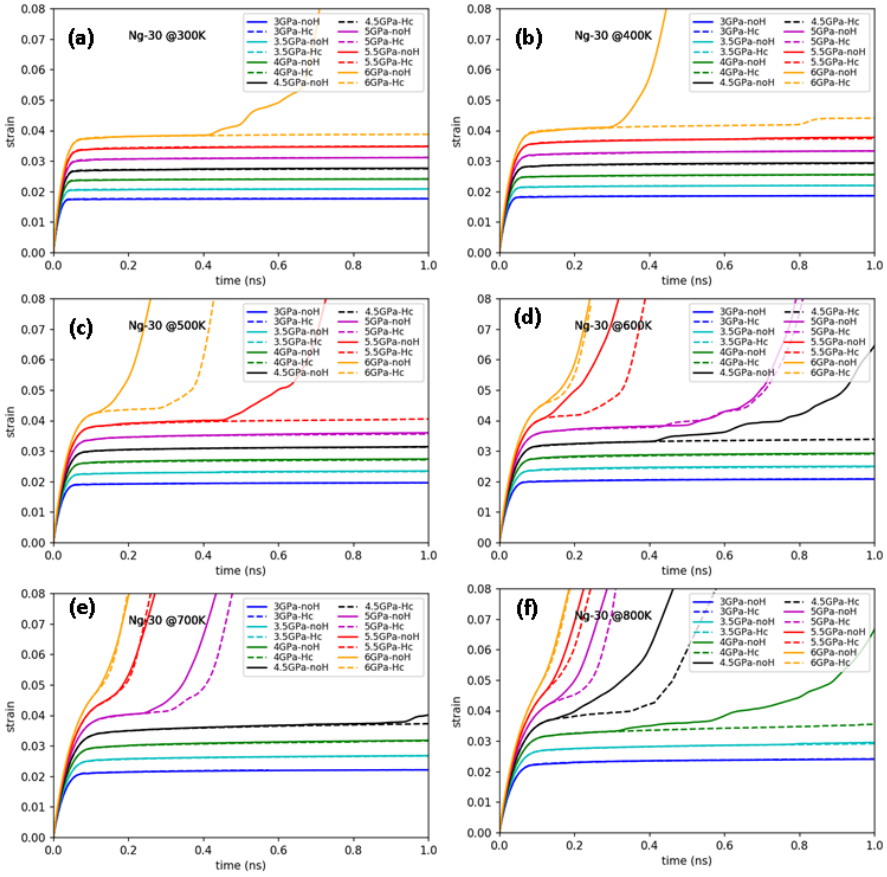

A2. The creep curves of the NG-30 at different temperatures and sustained stress.

Supplementary Materials for "Unveiling the role of hydrogen on the creep behaviors of nanograined α-Fe via molecular dynamics simulations"

Xiao-Ye Zhou[a], Ji-Hua Zhu[a*], Hong-Hui Wu[b*], Xu-Sheng Yang[c, d], Shuize Wang[b], Xinping Mao[b*]

[a] Guangdong Province Key Laboratory of Durability for Marine Civil Engineering, College of Civil and Transportation Engineering, Shenzhen University, Shenzhen, Guangdong 518060, PR China

[b] Beijing Advanced Innovation Center for Materials Genome Engineering, University of Science and Technology Beijing, Beijing 100083, China

[c] Advanced Manufacturing Technology Research Centre, Department of Industrial and Systems Engineering, The Hong Kong Polytechnic University, Hung Hom, Kowloon, Hong Kong

[d] Hong Kong Polytechnic University Shenzhen Research Institute, Shenzhen, China

Corresponding Authors

*Ji-Hua Zhu, E-mail: zhujh@szu.edu.cn

*Hong-Hui Wu, E-mail: wuhonghui@ustb.edu.cn

*Xinping Mao, E-mail: maoxinping@ustb.edu.cn

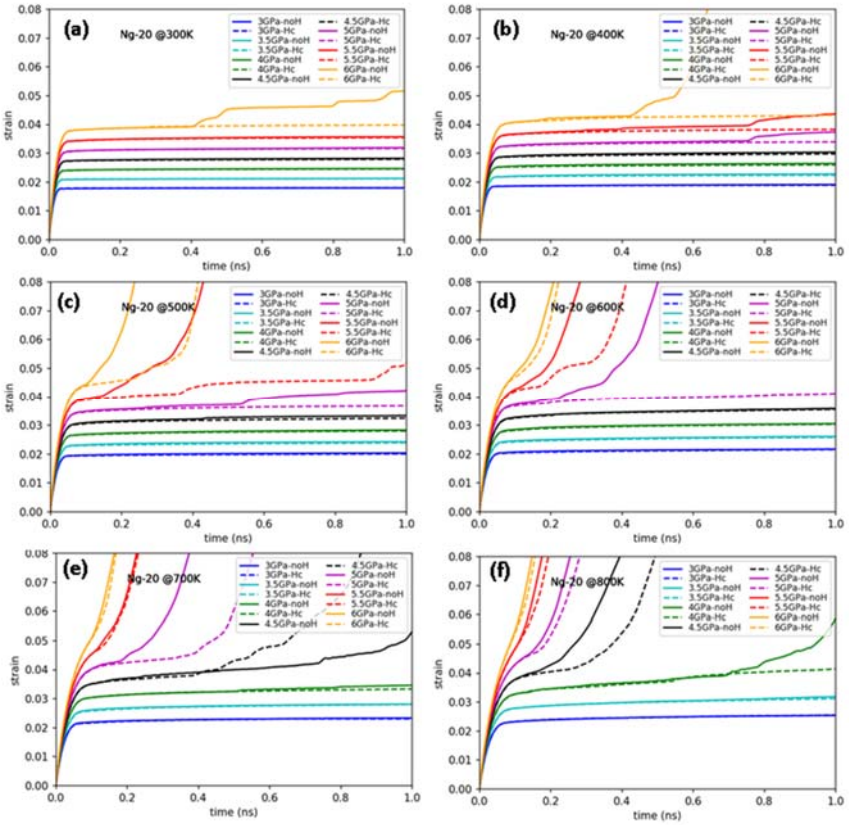

S1. The creep curves of the NG-20 at different temperatures and sustained stress.

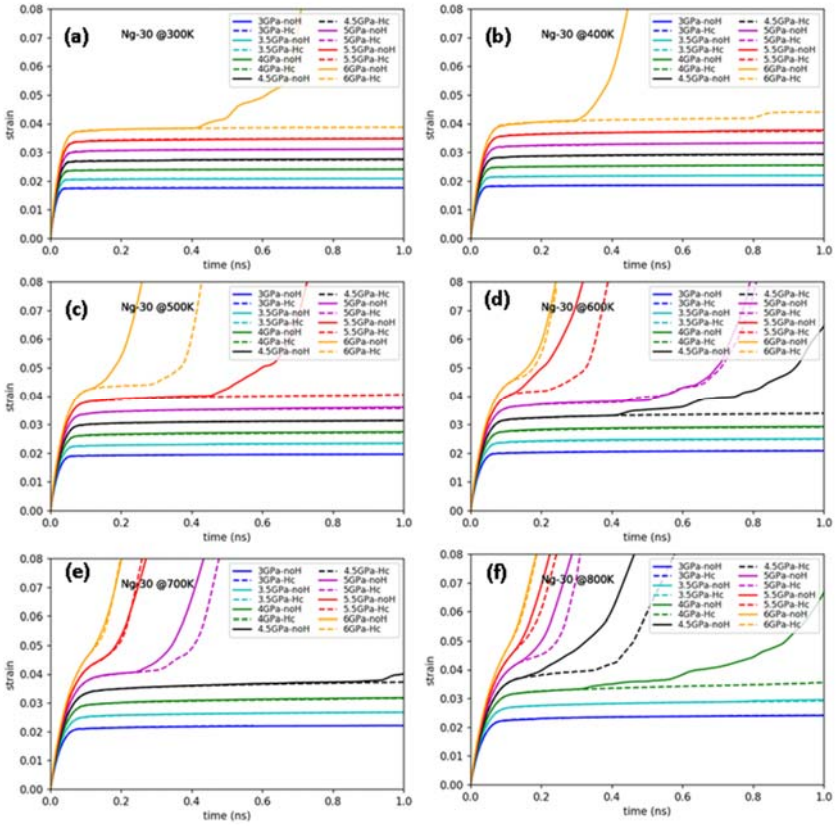

S2. The creep curves of the NG-30 at different temperatures and sustained stress.